Investigating the Effects of High Magnetic Fields on the Phase Stability of $Tl_2Ba_2Ca_2Cu_3O_{10-\delta}$ Superconductor

Belqees Hassan,[1*] Ali Alnakhlani[1] and Muhammad Abdulhafiz[2]

[1]Department of Physics, College of Science, Qassim University,
Buraydah 51452, Saudi Arabia
[2]Biological and Physical Sciences Department, Columbus State Community College,
Columbus, USA

[*]Corresponding author: B.Hassan@qu.edu.sa

ABSTRACT: *The standard superconducting oxides technique for synthesising superconducting oxides was applied under normal pressure to prepare the $Tl_2Ba_2Ca_2Cu_3O_{10-\delta}$ (Tl-2223) superconductor. It is found the optimal conditions and synthesis methods to achieve the formation and stability of the high phase Tl-2223, as well as the appropriate working ranges for the samples to obtain the best superconductor characteristics. The X-ray diffraction (XRD) analysis demonstrated the formation of the tetragonal phase of Tl-2223. The transition behaviour of sample was studied using high magnetic fields ranging from zero T to 10T. The results demonstrated an estimated critical magnetic field (Hc_2) of about 20T and a long coherence length of approximately 4 nm. The transition temperature of about 122 K and the direct current (DC) susceptibility of the superconductor were calculated. It was noted that with an increase in the applied magnetic field, both the transformation temperature and the DC susceptibility values decreased at T = 0 K. These findings provide important insights into the properties and behaviour of Tl-2223 under different conditions.*

Keywords: optimal conditions, stability, critical magnetic field, coherence length, susceptibility

1. INTRODUCTION

The Tl$_2$Ba$_2$Ca$_2$Cu$_3$O$_{10-\delta}$ (Tl-2223) superconductor is known for its high transition temperature (T$_c$), which exceeds the boiling point of liquid nitrogen. This characteristic makes it an attractive candidate for practical applications in areas such as energy transmission, power generation and magnetic resonance imaging (MRI). Additionally, its high critical current density and excellent flux pinning properties make it suitable for applications in superconducting magnets and high-field devices. At the transition width ($\Delta T = T_c - T_0$) between the critical T$_c$ and the zero resistance temperature (T$_0$), superconductivity can be obtained. The driving current and the applied magnetic field have an effect on the transition width.[1,2] When compared to low T$_c$ superconductors, the transition width may reach a value between 40K–50K.[3] High-temperature superconductors typically, exhibit this behaviour, where the resistance changes significantly, as the temperature drops until it reaches T$_0$. The applied magnetic field affects the superconductors' zero-resistance amplitude. The effect of a magnetic field on electrical resistance measurements reveals a plethora of details about the upper critical field, activation energy and vortex dynamics in type II superconductors.[4–6] Above T$_c$ (normal operating temperature), both small and moderate applied magnetic fields have no effect on electrical resistance data. The presence of a magnetic field, however, lowers the transition temperature and broadens the transition width below the transition (superconducting state). Temperature-dependent resistance (R-T curves) versus applied field are used to estimate the upper critical field $\mu_0 Hc_2(T)$. These fields are defined as those in which the temperature-dependent resistance at constant magnetic field $R[\mu_0 Hc_2(T)] = 0.9R_n$, where R$_n$ is the normal state resistance.[7–9] The intercept of $\mu_0 Hc_2(T)$ to zero in the temperature axis is taken as the direct $\mu_0 Hc_2(0)$.[10–13] The (Tl-2223) superconductor phase has been the focus of extensive research due to its unique properties and potential applications. Several studies have investigated the effects of high magnetic fields on the phase stability of Tl-2223 superconductor. The magnetoresistance behaviour of (TlF) x-substituted (Cu$_{0.5}$,Tl$_{0.5}$)Ba$_2$Ca$_2$Cu$_3$O$_{10-\delta}$ samples showed an increase in flux pinning energy with increasing F-substituting up to x = 0.1, then a decrease with increasing applied field.[14] The effect of an applied magnetic field on the transition behaviour of Tl$_m$Ba$_2$Ca$_{n-1}$Cu$_n$O$_{2n+2+\delta}$ superconductor was also studied, and it was observed that the transition width increased sharply with a slight increase in the magnetic field.[15] In (Cu$_{0.5}$Tl$_{0.5}$)Ba$_2$Ca$_3$(Cu$_{4-x}$Ti$_x$)O$_{12-\delta}$ superconductor samples, it was found that the critical current density J$_c$ was suppressed with an increased field, and the pinning strength increased with the concentration of T$_i$ doping.[16] The effect of nanosized Bi$_2$O$_3$ on the formation of the Tl$_2$Ba$_2$CaCu$_2$O$_8$ phase was studied, and it was observed that the transport critical current density was highest in the mixed phase sample with x = 0.1.[17] Pure phase Tl$_2$Ba$_2$Ca$_2$Cu$_3$O$_{10}$ films

with good superconducting properties were obtained using a triple post-annealing process, and the critical current densities reached 4.0 MA/cm^2 at 77K at self-field.[18] This work aims to build upon the previous results and advancements in this field, and contribute to the optimisation and characterisation of the Tl-2223 superconductor, with the ultimate goal of harnessing its full potential for practical applications in various fields. In this work, Tl-2223 samples were prepared using a solid-state reaction method and their superconducting characteristics were investigated.

2. EXPERIMENTAL DETAILS

The oxides used in this study were purchased from Sigma-Aldrich, to produce the desired quantities of Tl_2O_3, BaO_2, CaO and CuO with high purity of 99.95% for the preparation of the studied sample. The details of the Tl-2223 sample preparation process, as mentioned in the work by Hassan et al.[15,19] The powder was formed into a disc 1.5 cm in diameter and 0.2 cm thick. To prevent thallium evaporation during the process, the sample was wrapped in silver foil. To protect the furnace from potentially hazardous effects, the disc samples were placed horizontally in a stainless steel tube with a diameter of 1.5 cm and a length of 15 cm. The sealed tube was placed in a furnace and heated to 811°C at a rate of 6°C/min for 6 h before being cooled to room temperature at a rate of 0.5°C/min. The Tl-2223 superconducting material was annealed in a normal atmosphere at 500°C to improve its superconductivity properties.[20] The electrical resistance of the samples was measured using a standard four-point probe method with a Keithley 2400 SourceMeter. Temperature-dependent resistance and DC susceptibility measurements were performed using a LakeShore 7400 Series Superconducting Magnet System. The sample temperature was precisely controlled within 1 mK using a LabVIEW-controlled system that coordinated both the Keithley Source Meter and Lakeshore temperature controller. Measurements were taken over a temperature range of 10 K–300 K, with various applied magnetic fields of H = 0 T, 0.1 T, 0.25 T, 0.5 T, 1 T, 2 T, 4 T, 6 T, 8 T and 10 T.

3. RESULTS AND DISCUSSION

3.1 X-ray Diffraction

Based on X-ray powder diffraction (XRD) scanning operations, distinct and sharp diffractions were obtained as shows in Figure 1. The observed peaks correspond excellently with the tetragonal structure of the Tl-2223 phase, which

is characterised by the space group P4/mmm. The average values of the lattice parameters are, a = 3.77 Å and c = 37.5 Å. These parameters define the size and shape of the unit cell. The crystallite size of the superconducting compound Tl-2223 was calculated from XRD data using the Debye Scherer method.

$$D = \frac{K\lambda}{\beta\cos\theta} \qquad (1)$$

Where D is the average crystallite size (nm), K is the Scherrer constant, (K= 0.94), λ is the X-ray wavelength, (λ =1.5406 Å), β is the line broadening at full width at half maximum (FWHM) in radians, θ is the Bragg's angle in degrees. The average crystallite size was found to be 36.69 nm.
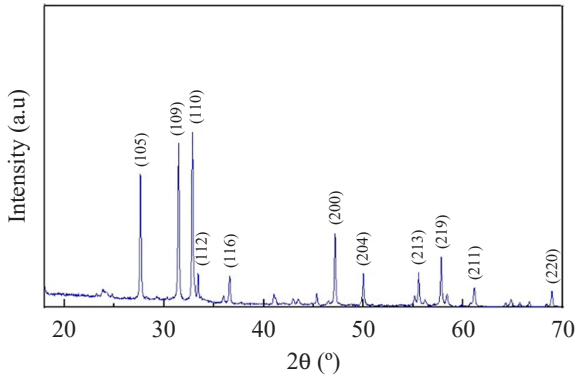

Figure 1: XRD spectrum of sample Tl-2223.

To further investigate the potential presence of microstrain, a Williamson-Hall (WH) analysis was performed. The WH plot Figure 2 showed a nearly horizontal linear relationship between βCosθ and 4Sinθ. This indicates that the contribution of microstrain to the peak broadening is very small, suggesting minimal lattice distortion or defects in the sample. The analysis yielded a microstrain value of 0.00057, and the crystallite size was determined to be 46.6 nm. The crystallite size calculated from the WH analysis is slightly larger than that obtained from the Scherer equation. This discrepancy can be attributed to the fact that the WH analysis accounts for the presence of microstrain, which is not considered in the Scherer equation. Microstrain arises from lattice distortions and defects within the material, leading to a broader diffraction peak and an apparent larger crystallite size when using the Scherer equation alone. The WH analysis provides a more accurate estimate of the crystallite size by accounting for both size and strain contributions to the peak broadening. The analysis yielded a crystallite size of 46.6 nm, which falls within the typical range observed for Tl-2223 superconductors, often exhibiting crystallite sizes less than 100 nm.[21,22]

This size range is often associated with enhanced superconducting properties, as nanometer-sized particles facilitate efficient current flow and reduce scattering. The small particle size in our sample is likely due to the precise manufacturing techniques and controlled crystal growth conditions employed during synthesis. Generally, nanometer-sized particles in superconducting materials, including Tl-2223, contribute to increasing the ability of the material to conduct electric current without resistance. The particle size for superconducting materials may vary depending on the precise manufacturing techniques and controlled crystal growth conditions employed during synthesis.
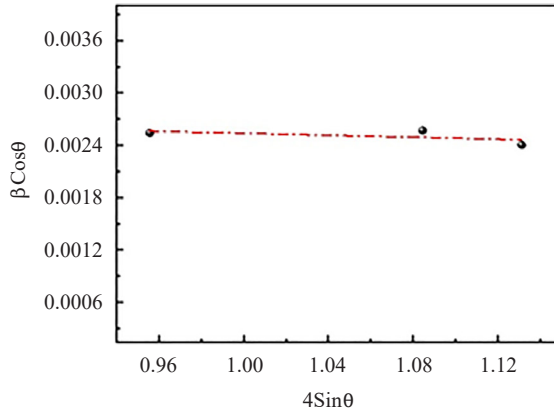

Figure 2: WH plot for Tl-2223 superconductor.

3.2   Effect of DC Magnetic Field and Normal State

Figure 3 illustrates the temperature dependence of the normalised resistance of the Tl-2223 sample. In Figure 3, one may distinguish two stages of the transition into the superconducting state in the curve of the resistance depended on the temperature. The high temperature region exhibits a quick drop in resistance of a few Kelvins starting at the onset temperature (T_c^{onset} = 122 K). In the low temperature region, the normalised resistance gradually decreases to zero as the temperature approaches T_0. This is thought to be due to the high temperature superconductors' granular structure and relatively short coherence length.[23] It is noted that the magnetic field H has no impact on the first stage of the transition (T: 300 K–112 K), as shown by Figure 3, where the resistance curves obtained at various magnetic field strengths overlap in the high temperature range. This could also include data on the spatial distribution of "strong" superconducting grains and "weak" superconducting boundaries. In the second stage (T:112 K–10 K), we observe that, for larger values of the magnetic field, the applied magnetic field causes a rise in the transition width ΔT.
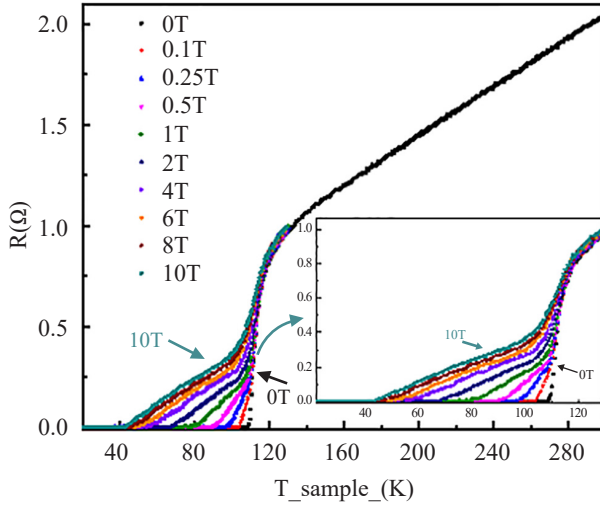
Figure 3: The temperature dependence of the normalised resistance for Tl-2223 under various magnetic fields.

The sample is metallic until 130 K, at which point resistance saturation begins to show. The temperature at which the resistance R is less than 10^{-4} Ω is known as the critical temperature, or $T_c^{offset} = 112$ K. The temperature difference between the temperatures measured at 90% and 10% of the normal state resistance R_n, the value of the resistance right before the superconducting transition, is known as the superconducting transition width, and it is equal to $\Delta T_c = 10$ K. In the inset of Figure 3, it can be seen that in the absence of magnetic fields, the resistance begins to decline at 122 K and disappears at 112 K. Above T_c, the resistance exhibits linear behaviour, and the Residual Resistance Ratio (RRR) is obtained, where RRR = R (300 K)/R(T_c) = 2.20, indicating that scattering becomes large at the onset temperature and demonstrating the good quality of the current sample. With an increasing magnetic field, the T_c gradually drops. However, at the same time that the $\Delta T_c [T_c(90\%)-T_c(10\%)]$ broadens, the T_c (R = 0) dramatically declines. The onset critical temperature T_c^{onset}, the T_0, the transition width ΔT_c for and the critical temperature T_c are listed in Table 1. The enlargement of the resistance transition area under a magnetic field across a broad temperature range below T_c, which has recently become an empirically well-established phenomenon, is one of the intriguing features of the high T_c superconductors. We note from this table that the obtained T_c is 122 K, and this value is slightly higher than the value obtained previously.[24]

Table 1: The different parameters for Tl-2223 sample

The onset critical temperature (K)	The zero resistance temperature (K)	The transition width (K)	The residual resistance ratio	The critical temperature (K)
T_c^{onset}	T_c^{offset}	ΔT_c	RRR	T_c
122	112	10	2.20	122

3.3 Determination of the Upper Critical Field

The upper critical field (Hc_2) can be determined experimentally using various techniques such as magnetisation, resistivity and specific heat measurements. One common method to determine Hc_2 is by measuring the temperature dependence of the resistivity under applied magnetic fields. Figure 4 shows the Hc_2 values for a Tl-2223 sample at different temperatures. The Hc_2 values decrease as the temperature increases. The Hc_2 (0) value is determined by extrapolating the graph to 0 K.
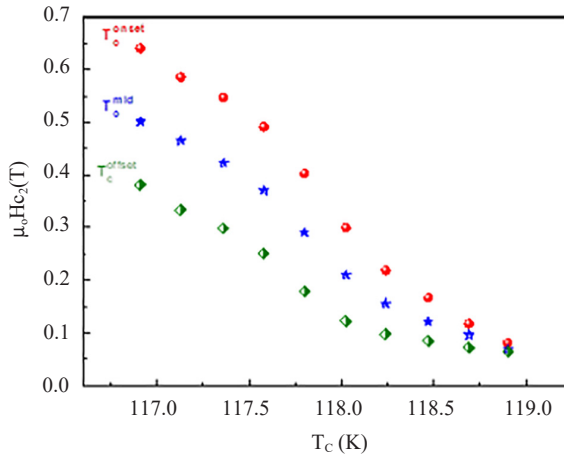

Figure 4: The temperature dependencies of upper critical field for Tl-2223 sample at three defined temperatures.

The Hc_2 in high T_c cuprate can be calculated using different percentages of normal state resistance, such as 90%, 50% and 10%, which correspond to the onset, mid-point and zero-resistance temperatures of the superconducting transition. T_c at (T = 0 K) is found to have values of T_c^{onset} (0) = 111.28 K, T_c^{onset} (0) = 111.28 K, T_c^{mid} (0) =110.71 K and T_c^{offset} (0) = 109.2 K. gives the relationship between temperature and the upper critical magnetic field:[25]

$$Hc_2(T) = Hc_2(0)\left(1 - \frac{T}{T_c}\right) \qquad (2)$$

To determine Hc$_2$ (0), use the extrapolation Hc$_2$ (T) to T = 0 K. At T$_c^{onset}$(0), T$_c^{mid}$(0) and T$_c^{offset}$(0), the slopes of μ$_o$Hc$_2$ are –0.255 T/K, –0.231 T/K and –0.218 T/K, respectively. The zero-field upper critical field Hc$_2$ (0) can also be calculated using the Werthamer-Helfand-Hohenberg formula:[26]

$$\mu_0 Hc_2(0) = -0.693 T_c \left(\frac{dHc_2}{dT} \right)_{T=T_c} \tag{3}$$

At zero temperature, the upper critical magnetic fields are estimated to be μ$_o$Hc$_2^{onset}$ = 20.1 T; μ$_o$Hc$_2^{mid}$ = 17.65 T and μ$_o$Hc$_2^{offset}$ = 16.95 T. Due to the difficulty in measuring the amount directly, the coherence length can be determined from the upper critical magnetic field at T = 0 K. The Ginzburg-Landau formula is used to determine the coherence lengths ξ(0) for T = 0 K:[27]

$$\xi(0) = \sqrt{\frac{\Phi_0}{2\pi\mu_0 Hc_2(T)}} \tag{4}$$

Where Φ_0 represents the magnetic flux quantum, which has a value of 2.07×10^{-15} Tm^2. This leads to ξ (0) of 40.5 Å, 43.2 Å and 44.1 Å for the data corresponding to the onset, the mid and the offset positions, respectively. The obtained values of parameter are listed in Table 2. The table shows that the upper critical field decrease as the transition temperature decreases. The high values of Hc$_2$ and ξ are apparently due to grain boundary effects from the polycrystalline sample. The highlights of this study is the estimation of Hc$_2$ and coherence length from the behaviour of electrical resistivity in magnetic fields. However, the estimated Hc$_2$ of about 20 T and the long coherence length of about 4 nm are exceptional values for a cuprate superconductor showing T$_c$ > 100 K. The reason for the values of Hc$_2$ and coherence length in the Tl-2223 superconductor is likely due to the presence of grain boundaries in the polycrystalline sample. Grain boundaries act as barriers to the superconducting current flow, and disrupts the smooth propagation of the superconducting wave function, leading to a decrease in ξ, the characteristic length over which cooper pairs can exist. This reduction in coherence length directly affects the Hc$_2$ by decreasing its value. A shorter coherence length leads to more closely spaced magnetic vortices within the material, increasing the disruption to the superconducting state and making the material more susceptible to magnetic field-induced suppression of superconductivity. Grain boundaries can have a significant effect on the physical properties of a material, including its superconducting properties. In the case of the Tl-2223 superconductor, the presence of grain boundaries may be causing an increase in the coherence length and a decrease in Hc$_2$ relative to what is typically observed in single crystal samples. This may be due to a reduction in the amount of disorder and defects at the grain boundaries, leading to a uniform distribution

of superconducting properties throughout the material. However, further studies would be needed to confirm this hypothesis. These values (Hc$_2$, ξ) agree well with experimentally determined values for typical high-temperature superconductors.[28]

Table 2: The critical temperature T$_c$, the upper critical magnetic field μ_0Hc$_2$ (0) and the coherence lengths ξ(0) of Tl-2223 sample

Physical parameters	90% onset(0)	50% mid(0)	10% offset(0)
T$_c$ (K)	111.28	110.71	109.20
μ_0Hc$_2$(0) (T)	20.10	17.65	16.95
ξ (0) (Å)	40.50	43.20	44.10

3.4   DC Magnetic Susceptibility Measurements

The diamagnetic behaviour of this sample was investigated by studying the DC magnetic susceptibility. The real part χ' and the imaginary part χ'' were illustrated in Figure 5. The onset critical temperature T$_c^{onset}$ was determined from the real part ($\chi'-$T) curve, A superconducting transition was clearly observed at T$_c^{onset}$ = 110 K, where that T$_c$ relating to the first negative value of χ', which corresponded to the intragrain superconductivity. The effect of magnetic field on ($\chi'-$T) exhibits a large broadening in the transition region.
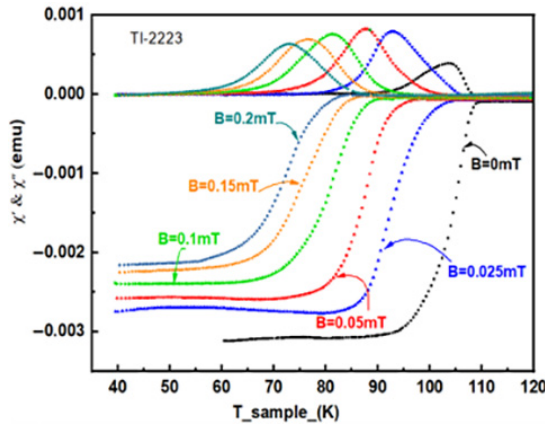

Figure 5: Temperature dependency of the real and imaginary components of susceptibility for Tl-2223 sample under various DC magnetic field.

The vortex dissipation that leads to the transition's broadening depends on the vortex pinning processes and vortex phase transformation. For illustrate, when a magnetic field is present, the presence of a vortex liquid phase in cuprates causes the superconducting transition to significantly broaden. The imaginary part, ($\chi''-$T) curve, is affected by the DC magnetic field, where the peak position

shifts to the lower temperature when the magnetic field increase to higher value. This suppression of the imaginary part can be attributed to the presence of strong pinning centers within the Tl-2223 superconductor. These pinning centres effectively immobilise or limit the movement of vortices even at higher magnetic fields, reducing their energy dissipation.[29] As a result, the imaginary part peak is suppressed or diminished. By comparing the critical temperature of the measurements taken we note that the onset critical temperatures obtained from the magnetic susceptibility χ' (T$_c^{onset}$ = 110 K) is lower than this value obtained from the resistance measurements (T$_c^{onset}$ = 122 K) for the studied sample. This can be explained as follows; a measurement of the magnetic susceptibility is a more typical variable of the thermodynamic state; and resistance, however, is simpler to measure and may provide better application guidance. The temperature T$_c^{onset}$ at which the resistance value equal to zero is reached typically happens at a little bit higher than the temperature at which its susceptibility equivalent occurs. Because each minuscule section of the superconductive material loses its resistance, R = 0 when one or more continuous superconducting channels exist between the measuring electrodes. On the other hand, diamagnetic measurements rely on macroscopic current loops to shield the magnetic field from a significant portion of the sample material, which happens when entire superconducting current channels are made feasible. The discrepancy in T$_c$ between electrical resistance and magnetic susceptibility measurements in the Tl-2223 sample likely arises from its polycrystalline structure. Grain boundaries, acting as weak links, interrupt superconducting current flow and hinder the formation of continuous superconducting pathways. The strength of inter-grain coupling is critical, with weak coupling reducing the diamagnetic response measured by susceptibility. However, even a few strong superconducting pathways can lead to a significant drop in resistance. This emphasises that understanding the sample's microstructure, including grain boundaries, is crucial for interpreting the superconducting properties of Tl-2223.

4.   CONCLUSION

The sample preparation method plays an important role in obtaining high-phase superconducting samples Tl-2223 and requires great control over all preparation conditions starting from the selection of materials and ending with obtaining the samples in their final form. In this study, at normal pressure, we investigated the superconducting properties of the Tl-2223 sample under various applied magnetic fields. Magnetic susceptibility and resistance measurements indicated onset resistance critical temperatures around 110 K and 122 K, respectively. XRD data and results indicate that Tl-2223 has a tetragonal crystal structure. The Hc$_2$, the coherence lengths, and the activation energy were investigated at T = 0 K.

5.　ACKNOWLEDGEMENTS

6.　REFERENCES

1.　Khosroabadi, H., Daadmehr, V. & Akhavan, M. (2003). Magnetic transport properties and Hall effect in $Gd_{1-x}Pr_xBa_2Cu_3O_{7-\delta}$ system. *Physica C Supercond.*, 384(1–2), 169–177. https://doi.org/10.1016/S0921-4534(02)01876-2

2.　Abou-Aly, A. I., Ibrahim, I. H. & Awad, R. (2000). Synthesis and characterization of the Indium-doped Tl-1223 phase. *J. Mater. Sci.*, 35, 2893–2896. https://doi.org/10.1023/A:1004719823976

3.　Lee, J. H., Lee, S. C. & Khim, Z. G. (1989). Noise measurement near the transition region in $YBa_2Cu_3O_{7-\delta}$ thin-film superconductor. *Phys. Rev. B.*, 40(10), 6806. https://doi.org/10.1103/PhysRevB.40.6806

4.　Schilbe, P. et al. (2003). Irreversibility fields of the high-Tc superconductors Hg-1212 and (Hg, Tl)-1212. *Physica C Supercond.*, 391(3), 298–304. https://doi.org/10.1016/S0921-4534(03)00958-4

5.　Awad, R. et al. (2001). Effect of magnetic field on the electrical resistance of Tl-1223 doped by Zn and Ni. *Physica B Condens. Matter*, 307(1–4), 72–77. https://doi.org/10.1016/S0921-4526(01)00971-1

6.　Ogale S. B. et al. (1995). Resistivity transitions in applied magnetic fields in epitaxial thin films of Fe- and Zn-doped $YBa_2Cu_3O_{7-\delta}$. *Phys. Rev. B*, 51(17), 11753. https://doi.org/10.1103/PhysRevB.51.11753

7.　Erdem, M. et al. (2011). Effect of Gd addition on the activation energies of Bi-2223 superconductor *Physica B Condens. Matter*, 406(3), 705 –709. https://doi.org/10.1016/j.physb.2010.12.008

8.　Çelik, Ş. et al. (2008). Investigation of the dependency of the upper critical magnetic field on the content x in $Y_{1-x}Yb_{x/2}Gd_{x/2}Ba_2Cu_3O_{7-y}$ superconducting structures. *J. Alloys Compd.*, 460(1–2), 79–82. https://doi.org/10.1016/j.jallcom.2007.06.037

9.　Attanasio, C. et al. (2004). Pinning energy and irreversibility line in superconducting $GdSr_2RuCu_2O_8$. *Physica C Supercond.*, 411(3–4),126–135. https://doi.org/10.1016/j.physc.2004.07.004

10.　Yadav, C. S. & Paulose, P. L. (2009). Upper critical field, lower critical field and critical current density of $FeTe_{0.60}Se_{0.40}$ single crystals. *New J. Phys.*, 11(10), 103046. https://doi.org/10.1088/1367-2630/11/10/103046

11.　Triscone, G., Junod, A. & Gladyshevskii, R. E. (1996). Magnetic and thermal properties of the 116 K superconductor Tl-1223. Physica *C Supercond.*, 264(3–4), 233–249. https://doi.org/10.1016/0921-4534(96)00262-6

12.　Tanaka S. (2006). High-temperature superconductivity. *Jpn. J. Appl. Phys.*, 45, 9011. https://doi.org/10.1143/JJAP.45.9011

13.   Liu, S. L. et al. (2005). The effective activation energy U$_{eff}$ (T,B,J) in Hg-1223 single phase superconductors. *Solid State Commun.*, 133(9), 615–620. https://doi.org/10.1016/j.ssc.2004.10.034

14.   Hassan, M. S. et al. (2022). Effects of Thallium fluoride substitution on the flux pinning energies of (Cu$_{0.5}$, Tl$_{0.5}$)Ba$_2$Ca$_2$Cu$_3$O$_{10-\delta}$ superconductors. *Appl. Phys. A*, 128, 1078. https://doi.org/10.1007/s00339-022-06170-z

15.   Hassan, B., Alnakhlani, A. & Abdulhafiz, M. (2021). Effects of Tl content and magnetic field on phase formation of Tl$_m$Ba$_2$Ca$_{n-1}$Cu$_n$O$_{2n+2+\delta}$ (m=1 and 2, n=4) superconductors. *Physica C Supercond.*, 586, 1353874. https://doi.org/10.1016/j.physc.2021.1353874

16.   Amna, I. et al. (2022). Infield magnetic measurements of (Cu$_{0.5}$Tl$_{0.5}$)Ba$_2$Ca$_3$(Cu$_{4-x}$Ti$_x$)O$_{12-\delta}$ (x=0, 0.25, 0.50, 0.75) samples. *Low Temp. Phys.*, 48, 193–199. https://doi.org/10.1063/10.0009536

17.   Dabaa, I. M. O. & Abd-Shukor, R. (2017). Phase formation and transport critical current density of Tl$_2$Ba$_2$CaCu$_2$O$_8$ superconductor with nano Bi$_2$O$_3$. *Solid State Phenom.*, 268, 320–324. https://doi.org/10.4028/www.scientific.net/SSP.268.320

18.   Xie, W. et al. (2014). Formation of epitaxial Tl$_2$Ba$_2$ Ca$_2$Cu$_3$O$_{10}$ superconducting films by dc-magnetron sputtering and triple post-annealing method. *Chinese Phys. B*, 23(7), 077401. https://doi.org/10.1088/1674-1056/23/7/077401

19.   Hassan, B. et al. (2016). Influence of KMnO$_4$ substitution on the structural and transport properties of Tl$_2$Ba$_2$Ca(Cu$_{1-x}$R$_x$)$_2$O$_{\delta+6}$ System, *J. Phys. Sci.*, 27(3), 13–24. https://doi.org/10.21315/jps2016.27.3.2

20.   Alnakhlani, A. et al. (2019). Effect of preparation and annealing temperature on the properties of (Hg, Tl)-2223 superconductor. *J. Phys. Sci.*, 30(1), 1–9. https://doi.org/10.21315/jps2019.30.1.6

21.   Vinila, V. S. et al. (2014). XRD studies on nano crystalline ceramic superconductor PbSrCaCuO at different treating temperatures. *Crystal Struct. Theory Appl.*, 3(1), 1–9. https://doi.org/10.4236/csta.2014.31001

22.   Blanco-Gutiérrez, V., Torralvo-Fernández, M. J. & Alario-Franco, M. Á. (2017). Particle size effect on the superconducting properties of YBa$_2$Cu$_3$O$_{7-x}$ particles. *Dalton Trans.*, 46(35), 11698–11703. https://doi.org/10.1039/C7DT01974B

23.   Tinkham M. (1988). Resistive transition of high-temperature superconductors. *Phys. Rev. Lett.*, 61(14), 1658. https://doi.org/10.1103/PhysRevLett.61.1658

24.   Khurram, A. A. & Khan, N. A. (2010). A search for a low anisotropic superconductor. *J. Electromagn. Anal. Appl.*, 2(2), 1387. https://doi.org/10.4236/jemaa.2010.22010

25.   Shigeta, I. et al. (2003). Temperature and field dependence of magnetization of MgB$_2$ polycrystals. *Physica C Supercond.*, 392–396(1), 359–363. https://doi.org/10.1016/S0921-4534(03)01049-9

26.   Werthamer, N. R., Helfand, E. & Hohenberg, P. C. (1966). Temperature and purity dependence of the superconducting critical field, Hc$_2$. III. Electron spin and spin-orbit effects. *Phys. Rev.*, 147(1), 295. https://doi.org/10.1103/PhysRev.147.295

27.   Yildirim, G. (2018). Formation of artificial flux pinning centers in Bi-2223 cuprate superconductor with Ni impurities and enhanced resistant to thermal fluxon motions of correlated 2D pancake vortices in new matrix. *J. Alloys Compd.*, 745, 100–110. https://doi.org/10.1016/j.jallcom.2018.02.187

28.   Hassan, B. et al. (2015). New method for determining the lower and upper critical magnetic field in Tl-2234 superconductor. *Aust. J. Basic Appl. Sci.*, 9(2), 34–39.

29.   Eley, S., Glatz, A. & Willa, R. (2021). Challenges and transformative opportunities in superconductor vortex physics. *J. Appl. Phys.*, 130, 050901. https://doi.org/10.1063/5.0055611